crystals

MDPI

Article

Application of La-Doped $SrTiO_3$ in Advanced Metal-Supported Solid Oxide Fuel Cells

Sabrina Presto [1], Antonio Barbucci [1,2], Maria Paola Carpanese [1,2], Feng Han [3], Rémi Costa [3] and Massimo Viviani [1,*]

1 Institute of Condensed Matter Chemistry and Energy Technologies (ICMATE), National Council of Research (CNR), c/o DICCA-UNIGE, Via all'Opera Pia 15, 16145 Genova, Italy; sabrina.presto@cnr.it (S.P.); barbucci@unige.it (A.B.); carpanese@unige.it (M.P.C.)

2 Department of Chemical, Civil and Environmental Engineering, DICCA-UNIGE, Via all'Opera Pia 15, 16145 Genova, Italy

3 Deutsches Zentrum für Luft- und Raumfahrt e.V. (DLR), German Aerospace Center, Institute of Engineering Thermodynamics—Electrochemical Energy Technology, Pfaffenwaldring 38-40, 70569 Stuttgart, Germany; Feng.Han@dlr.de (F.H.); remi.costa@dlr.de (R.C.)

* Correspondence: massimo.viviani@cnr.it; Tel.: +39-010-353-6025

Received: 31 January 2018; Accepted: 10 March 2018; Published: 13 March 2018

Abstract: Composite materials frequently allow the drawbacks of single components to be overcome thanks to a synergistic combination of material- and structure-specific features, leading to enhanced and also new properties. This is the case of a metallic-ceramic composite, a nickel-chromium-aluminum (NiCrAl) foam impregnated with La-doped Strontium Titanate (LST). This particular cermet has very interesting properties that can be used in different fields of application, namely: mechanical robustness provided by the metal foam; and chemical stability in harsh conditions of temperature and atmosphere by promotion of a thin protective layer of alumina (Al_2O_3); high electronic conductivity given by a percolating ceramic conducting phase, i.e., La-doped Strontium Titanate. In this paper, its application as a current collector in a metal-supported Solid Oxide Fuel Cells (SOFC) was studied. Firstly, the electronic properties of different compositions, stoichiometric and under stoichiometric, of LST were analyzed to choose the best one in terms of conductivity and phase purity. Then, LST chemical stability was studied in the presence of Al_2O_3 at different temperatures, gas compositions and aging times. Finally, stability and conductivity of LST-impregnated NiCrAl foam composite materials were measured, and LST was found to be fully compatible with the NiCrAl foam, as no reactions were detected in oxidizing and reducing atmosphere after up to 300 h operation at 750 °C and 900 °C between the Al_2O_3 layer and LST. Results showed that the composite is suitable as a current collector in innovative designs of metal-supported SOFC, like the Evolve cell, in which the metallic part is supposed not only to provide the structural stability to the cell, but also to play the role of current collector due to the impregnation of ceramic material.

Keywords: La-doped $SrTiO_3$; Solid Oxide Fuel Cells; electronic conductivity; impregnation; redox cycle; current collector; metal foam

1. Introduction

Solid Oxide Fuel Cells (SOFC) are one of the most efficient and environmentally friendly technologies available for generating power from hydrogen, natural gas, and other renewable fuels [1,2]. The challenges in the commercialization of SOFC are to reduce cost and increase the reliability of the system. Enormous research efforts are being directed towards lowering the temperature of SOFC from 1000 °C to below 800 °C and to reducing the startup time and reliability for portable power applications and transportation [3]. To achieve good performances, attention must be paid to optimization

strategies [4], and among these, to materials, geometrical aspects and design. SOFC are categorized into two major types, planar and tubular [5], the former being more promising at the moment. Technical parameters that can influence the processes of production of planar SOFC and, indirectly, their performance, have also been reported in literature [6]. Several designs of planar fuel cells have been reported: anode- or cathode-supported [7]; dual membrane [8,9], which is based on properties of a mixed anionic and protonic conductor used as a central membrane; electrolyte-supported cells in symmetrical configuration [10], which are very useful as reversible solid oxide cells; and metal-supported [11].

Metal-supported SOFC offer an alternative to conventional electrode- and electrolyte-supported cells, with some important advantages like the use of cheaper materials, enhanced mechanical stability to thermal cycling and temperature gradients, and manufacturability benefits.

The main obstacles in SOFC fabrication on porous Fe-Cr steel alloy supports are the constraints on sintering conditions due to high-temperature corrosion of the metal support, decomposition of the cathode materials in inert or reducing atmosphere, and the diffusion of Fe, Cr, and Ni between the ferritic Fe-Cr steel and nickel-containing anode.

To overcome these issues, several processing techniques have been proposed. The infiltration of active materials into pre-sintered porous metallic structures at relatively low temperature has been reported to ensure good performance and protection of the metallic structure. Ni-$Ce_{0.8}Sm_{0.2}O_{2-\delta}$ mixtures [12], Nb-doped $SrTiO_3$ [13], and Mo-doped $SrFeO_{3-\delta}$ [14] have been successfully employed as alternative electrocatalysts to the standard Ni-YSZ anodic composite, which exhibits excellent catalytic activity and current collection, but also suffers from serious limitations, such as Ni sintering, carbon deposition, sulphur poisoning, and low tolerance to redox cycles [15,16]. Additionally, alternative designs have been proposed, including the deposition of a protective La-doped $SrTiO_3$ layer between the metal support-active anode and the electrolyte layers, minimizing the Ni reaction with YSZ at sintering temperature [17].

An innovative approach was developed [18,19] in which the so called "Evolve" cell relies on a supporting current collector made of a ceramic-metal composite in the form of a metallic foam (0.6–1 mm thickness) impregnated with conductive ceramics. The metallic foam is a Ni-Cr-Al, and is supposed to provide structural stability to the cell and also to promote the formation of a thin continuous layer of Al_2O_3 during thermal processing in air. The coating is expected to enhance chemical stability, particularly avoiding Cr migration towards the active anode layer. Robustness against sulphur poisoning and thermal cycling is expected to increase significantly.

The main advantages of this oxidized structure are in its thermal stability and its ability to slow down the oxidation kinetics of the underlying metal in case of contact with an oxidant environment during the stack operation. The backbone of oxidized metal is then impregnated with conducting ceramics, such as La-doped Strontium Titanate, $La_{1-x}Sr_xTiO_3$ (LST), which leads to a percolating electron conducting phase.

Among the numerous other perovskite systems that have been explored, those containing Titanium continue to attract attention, because Ti remains mixed-valent Ti^{4+}/Ti^{3+} in the reducing atmosphere at the anode, and this redox couple can accept electrons from a hydrocarbon or H_2, thus promoting their dissociation. Because the formation of Ti^{3+} is favored by the reducing conditions, the atmosphere used during the sintering stage plays a crucial role in determining the final properties of these materials. Usually, the higher the sintering temperature and the stronger the reducing conditions, the higher the final conductivity will be, because of the higher concentration of Ti^{4+}/Ti^{3+} couples created. LST exhibits n-type semiconducting behavior when it is donor-doped and/or exposed to a reducing atmosphere. Lanthanum is a good donor dopant because the La^{3+} ionic radius (0.132 nm, CN XII) is similar to that of Sr^{2+} (0.140 nm, CN XII). Under oxidizing conditions, the compensation occurs due to the formation of Sr vacancies in the lattice, coupled with the formation of SrO layers within the structure. Under reducing conditions, Sr vacancies and SrO layers are eliminated, and the charge compensation for La^{3+} ions becomes electronic through the formation of electrons in the conduction band, i.e., conversion of Ti^{4+} to Ti^{3+} [20]. Because of its electrical properties and chemical

stability, this material is also considered promising for use in SOFC anodes [21], when it is either A- or B-site donor-doped [22–25], when mixed with other materials [26–28], under-stoichiometric compositions on site A [29] or A and B co-doped [30].

Oxygen-deficient compositions can be obtained by doping on the B-site with a cation of lower valence than the valence of the nominal B-site ion or by reducing a stoichiometric composition. The first approach led to the discovery of the compound with the highest known oxide ionic conductivity, $La_{1-x}Sr_xGa_{1-y}Mg_yO_{3-\delta}$ [31,32]. A-site deficiency has recently been used in various systems to prepare materials that are suitable for SOFC anodes. $La_xSr_{1-(3x/2)}TiO_3$ compositions sintered in air have been shown to exhibit conductivity values up to 7 S cm^{-1} upon reduction at 930 °C and $pO_2 = 10^{-20}$ atm [33,34]. The optimized composition of $La_{0.08}Sr_{0.86}TiO_{3-\delta}$ presents a conductivity of 82 S cm^{-1} at $pO_2 = 10^{-19}$ atm and 800 °C, after being pre-reduced in 7% H_2/Ar at 1400 °C, [35,36], which does not greatly increase when further doped on the B-site [37]. The effect of A-site deficiency has also been found to increase the electronic conduction of $Sr_{1-x}TiO_3$ under reducing conditions [38]; however, the increase is not significant, and phase segregation was also observed [39].

The aim of this paper is to study the thermal/chemical stability of LST-impregnated NiCrAl foam, a potential candidate as current collector for a metal-supported SOFC, under typical operative temperature and atmosphere conditions after up to 300 h operation and to measure its conductivity. For this purpose, the reduction of LST-based electron conducting ceramics was studied for several compositions, both stoichiometric and under-stoichiometric. LST-impregnated foams were also investigated in terms of their microstructural and chemical stability. LST was found to be fully compatible with the NiCrAl foam, as no reactions were detected between the Al_2O_3 layer and LST in oxidizing and reducing atmosphere after up to 300 h operation at 750 °C and 900 °C. Results showed that the composite is suitable as support in the innovative design of metal-supported Solid Oxide Fuel Cells (SOFC), in which the metallic part is supposed not only to provide structural stability to the cell, but also to play the role of current collector due to the impregnation of ceramic material.

2. Materials and Methods

In Table 1, the composition, synthesis method, and processing of the prepared and tested LST ceramics and impregnated foams are reported, for clarity. Details of each sample are also given in the text.

Table 1. List of prepared and tested LST samples. SSR = solid state reaction, SP = Spray Pyrolysis.

Name	Nominal Composition	Synthesis Route	Processing	Testing
LST185	$La_{0.1}Sr_{0.85}TiO_3$	SSR, 900 °C Air	Sintering: 1450 °C 12 h Air / Reduction:1450 °C 24 h Ar/H2	DC conductivity and Redox
LST27	$La_{0.2}Sr_{0.7}TiO_3$	SSR, 900 °C Air	Sintering: 1450 °C 12 h Air / Reduction:1450 °C 24 h Ar/H2	DC conductivity and Redox
LST-c	$La_{0.1}Sr_{0.9}TiO_3$	SP	Sintering: 1450 °C 12 h H_2	DC conductivity
LST-p-120	$La_{0.1}Sr_{0.9}TiO_3$ + graphite (40 vol %)	SP	Sintering: 1200 °C 12 h Air / Reduction: 1000 °C 24 h H_2	DC conductivity and Redox
LST-Al-mix	$La_{0.1}Sr_{0.9}TiO_3$ + Al_2O_3 (1:1 mol.)	SP	Calcination: 700-800-900-1000 °C 24 h	-
LST-Al-core	$La_{0.1}Sr_{0.9}TiO_3$ + Al_2O_3 pre-sintered (1600 °C) pellet	SP	Calcination: 700-800-900-1000 °C 24 h	-
Current collector	LST-c impregnated NiCrAl foam	SP	Reported in ref 18	DC conductivity and Redox

2.1. Powders and Pellets

A-site deficient LST powders, namely LST185 and LST27, as reported in Table 1, were prepared by solid-state reaction of the following precursors: $SrCO_3$ (grade HP, Solvay Bario e Derivati, Massa, Italy), TiO_2 (grade Aeroxide TiO_2 P 25, Evonik Degussa GmbH, Hanau, Germany), $La(OH)_3$, prepared by hydrolysis of an aqueous solution of $La(NO_3)_3 \cdot 4H_2O$ (Aldrich, 99.9%) with concentrated ammonia (Fluka, 25 wt %) and a solution of ammonium polyacrylate (Acros Chimica, MW 2000) as dispersant. The method consisted of the following steps: mixing and homogenizing for 24 h in stabilized zirconia media, freeze drying, sieving, and finally calcination of powder for 2 h at 900 °C in air. This temperature was chosen after various attempts to obtain a single LST phase powder.

A commercial LST powder (Ceramic Powder Technology AS, Heimdal, Norway), LST-c, with 10% at of La and prepared by spray pyrolysis, was also studied for comparison. LST powders were pelletized by a uniaxial pressing procedure and sintered at 1450 °C, in Ar-H_2 (5% of H_2) or air and then reduced at different temperatures as reported in Table 1. In some cases, graphite (Timcal Timerex, KS6) was added to the LST powder before pressing to obtain a porous material. Pt (Metalor, Birmingham-UK Pt ink) electrodes were brushed on the plane surfaces of sintered pellets and then cured at 1000 °C under the same atmosphere used for sintering.

To study the inter-material reactivity and compatibility of LST and Al_2O_3 materials, two different types of pellets were prepared, starting from LST-c and Alumina (Baikowski, batch 1134N) powders:

1. LST-Al-mix, obtained by mixing powders by water-based ball milling in stabilized zirconia balls, freeze drying, sieving, uni-axial pressing of pellet and calcination at 700–800–900–1000 °C for 24 h.
2. LST-Al-core, obtained by incorporating (uni-axial pressing) a pre-sintered (1600 °C) fully dense Alumina core in a LST pellet, and then calcination at 700–800–900–1000 °C for 24 h.

2.2. LST-Impregnated NiCrAl Foams

A NiCrAl standard foam (NiCrAl #1) from Alantum Europe GmbH, with an open cell size of about 450 µm was used as an alumina-forming alloy, in the form of sheets with 1.6 mm thickness. Square samples of 50 × 50 mm were cut from these sheets and impregnated with the LST-c slurry and fired in air at 1000 °C to obtain a current collector. The pore size of the substrates was reduced to 200 nm through the impregnation of LST ceramic into the metal foam. The details of impregnation are reported elsewhere [19].

2.3. Characterizations

Powders, pellets and impregnated foams (current collector) before and after reduction, and before and after thermal treatment and electrical characterization were analyzed by X-ray diffraction (CubiX, Panalytical) and Scanning Electron Microscopy (1450VP, LEO) to observe phase purity, microstructure and any degradation effect. XRD profiles were analyzed by the Rietveld method, as implemented in the FullProf software. The chemical composition was also confirmed, and element migration was studied by an energy-dispersive electron microprobe (INCA 300, Oxford Instruments). The electrical properties were studied with a 2-electrodes–4-wires set-up (ProboStat, NorECs AS, interfaced with a Solartron SI 1286 Potentiostat) both in air and in H_2 at different operative temperature and during redox cycles.

3. Results

3.1. LST Ceramics

3.1.1. Structural and Microstructural Properties

Phase purity of samples LST27, LST185 and LST-c was checked by XRD on ceramics sintered at 1450 °C for 12 h. In order to study the structural stability of A-site deficient compositions in reducing conditions, XRD was repeated after treatment at 1450 °C for 24 h under Ar-H_2 (5% of H_2). Results are reported in Figure 1 for all compositions, with Rietveld Refinement.

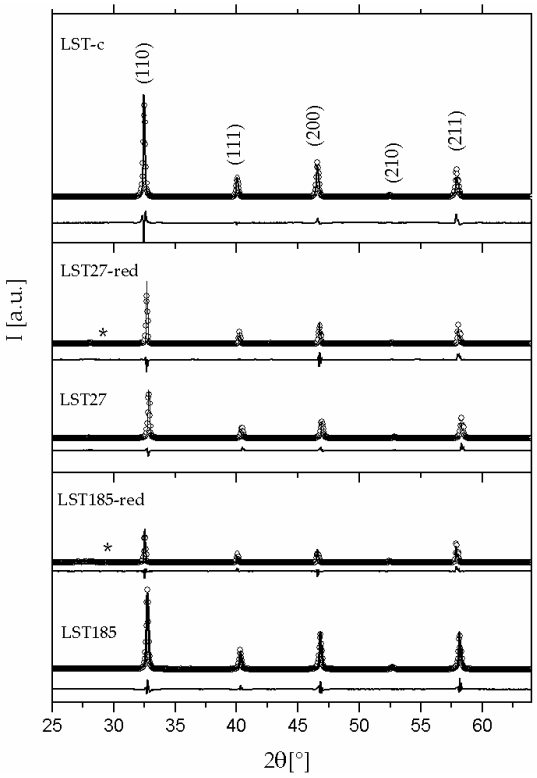

Figure 1. XRD patterns and Rietveld refinement of as-sintered and reduced LST samples, as indicated in labels. Residuals and Miller indexes of principal phase are also reported. (*) indicates major reflection of the $La_2Ti_2O_7$ secondary phase.

As-sintered materials are single cubic-phase, $SrTiO_3$-type (JCPDS card No. 86-179). Nevertheless, after reduction, some secondary phases, mostly $La_2Ti_2O_7$, are formed in LST27 and LST185 samples. The lattice parameters, and some reliability factors of Rietveld Refinement, are summarized in Table 2. Refinement, for reduced samples, was performed by also considering the secondary phase. From this table, it can be observed that lattice parameter increases with reduction. This behavior is in good agreement with previous results [24] and is due to partial reduction of Ti^{4+} to Ti^{3+}.

Table 2. Rietveld refined parameters of patterns reported in Figure 1.

Sample	Lattice Parameter (Å)	χ^2	R_B	R_F
LST-c	3.89767	1.72	6.11	3.01
LST185	3.90038	4.20	6.28	3.30
LST185-red	3.90712	8.12	17.5	11.2
LST27	3.89503	5.5	8.15	4.15
LST27-red	3.90551	7.53	12.7	6.48

Such phases were also detected by SEM, for LST185 and LST27 as separate darker intergranular areas (Figure 2b–d). EDX analysis, reported in Table 3, confirmed that dark grey zones correspond to Ti-rich phases, in which there is a depletion of Sr compared to the main phase. No defects were visible in the sample LST-c.

Table 3. Results of EDX analysis performed on reduced samples, as reported in Figure 2.

LST185-Red	O/Ti	Ti/(Sr+La)	La/Sr
Spectrum 1	3.44	0.97	41
Spectrum 2	2.92	1.01	0.12
LST27-Red	**O/Ti**	**Ti/(Sr+La)**	**La/Sr**
Spectrum 1	3.58	0.94	30
Spectrum 2	2.95	0.97	0.12
LST-c	**O/Ti**	**Ti/(Sr+La)**	**La/Sr**
Spectrum 1	3.10	0.94	0.12
Spectrum 2	2.96	0.98	0.13

Grain growth is coherently more evident in the sample containing 20 at % of La. In fact, average grain size is about 10 µm in LST27 and about 1 µm in LST185. LST-c showed a broader grain size distribution between about 1–4 µm which can be attributed to the different synthesis method used. In general, all samples show a high-density microstructure, even if, in the A-site-deficient samples, some intergranular voids are present, due to the fast grain growth process; such defects are typical in this type of sample and can be reduced by a fine tuning of the sintering process. Density was also measured by Archimedes' method, and a relative value of 96–97% for all ceramic materials was obtained.

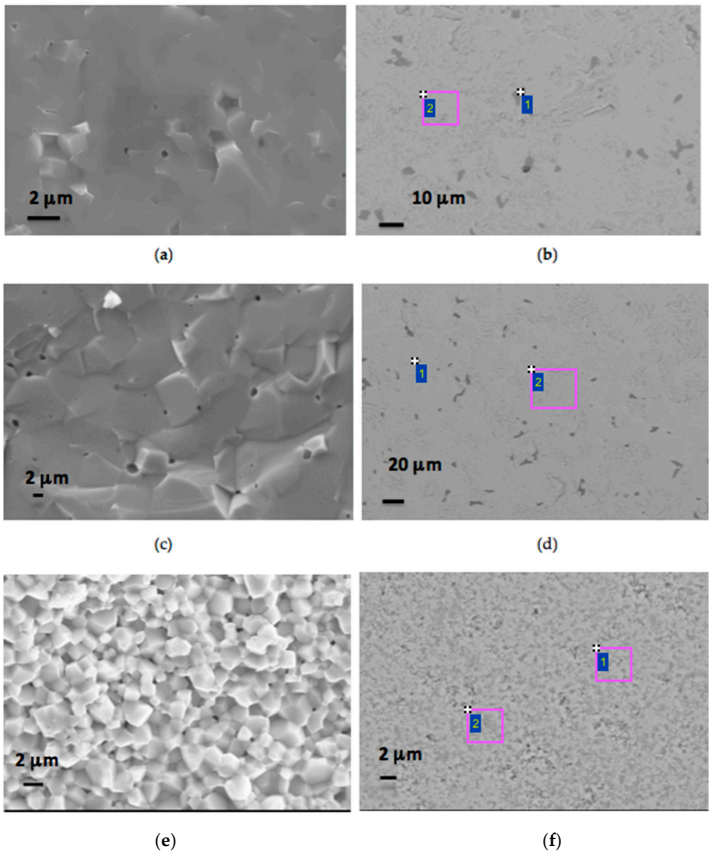

Figure 2. Microstructures obtained by SEM: SE image on fracture of as-sintered LST185 (**a**), LST27 (**c**) and LST-c (**e**); BSE image on cross section of reduced LST185 (**b**), LST27 (**d**) and of as-sintered LST-c (**f**).

3.1.2. Electrical Properties

In Figure 3, conductivity of oxidized ceramics, LST185 and LST27, measured in air is reported. LST-c was not measured in oxygen because it was sintered in Ar-H_2 to avoid strontium oxide segregation at the grain boundary, which could limit conductivity processes. A-site-deficient samples show thermally activated conduction as indicated by Arrhenius plot and low conductivity. Activation energy is 1.1 eV in LST185 sample, higher than 0.7 eV of LST27, possibly due to the prevailing grain boundary resistance given by the higher density of grain boundaries in the structure.

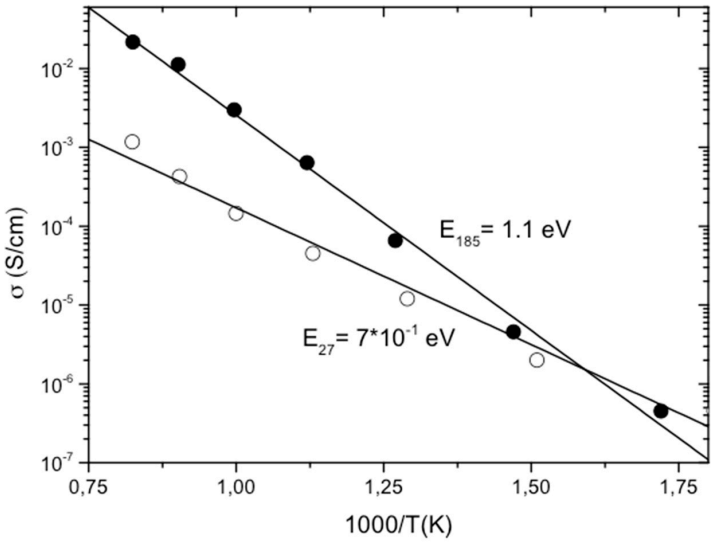

Figure 3. Arrhenius plot of total conductivity measured in air on oxidized samples (o) LST27, and (•) LST185.

After reduction, the conductivity was increased for both A-site-deficient samples (Figure 4), being higher for the LST27 sample. However, when compared to $Sr_{0.9}La_{0.1}TiO_3$ prepared by spray pyrolysis, conductivity appeared considerably limited. This result might be attributed to the secondary phases, which partially deplete the La concentration in the perovskite and also introduce a resistive phase in the volume. In addition, differences can be introduced by synthesis routes, i.e., by chemical homogeneity and the particle size of powders.

The effect of atmospheric composition on conducting properties was investigated by simulating RedOx cycles at fixed temperature on porous sample of LST-c, which showed higher conductivity and was chosen as the best powder to impregnate the NiCrAl foams and to study the composite material as a possible candidate for being a current collector in a metal-supported fuel cell.

As the main function of LST ceramics is to act as electronic conductor within the current collector and the active anode, its conductivity under reducing conditions is the most important quantity to check for practical use. However, the kinetics of transition from the oxidized non-conducting to the reduced conducting state is also of great importance and must be taken into account for the optimization of the current collector functionality.

At microscopic level, the oxidation (reduction) of LST involves two phenomena, which are the inbound (outbound) solid state diffusion of oxide ions and the surface exchange between solid and gas phases. The former is the limiting step; therefore, the kinetics of RedOx transitions is macroscopically determined by the microstructure, i.e., by the gas permeation through the LST network structure. The apparent conductivity is reported in Figure 5 for the sample sintered at 1200 °C (LST-p-120).

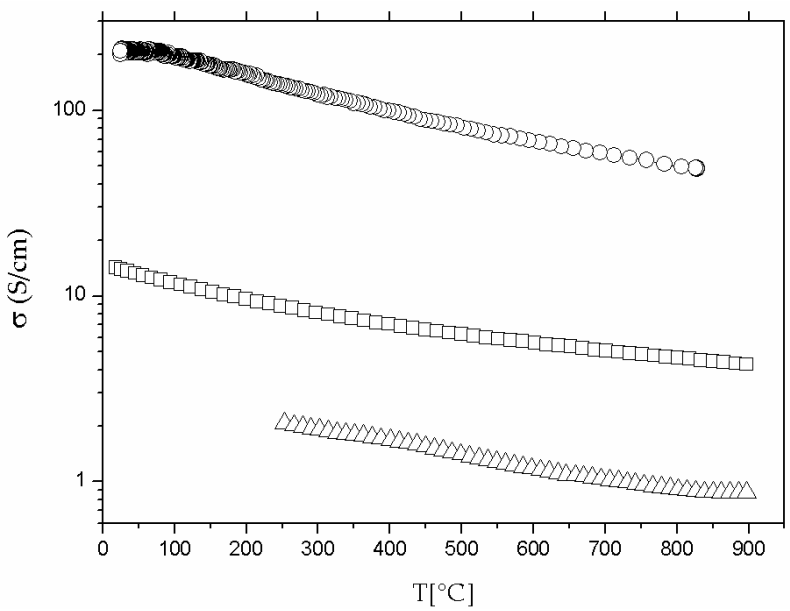

Figure 4. Conductivity as function of temperature, measured in hydrogen on sample (o) LST-c, and after reduction on samples (□) LST27 and (Δ) LST185.

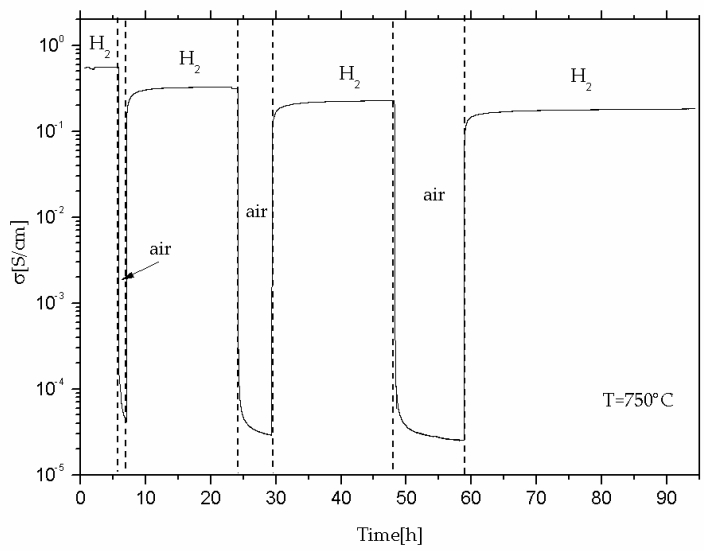

Figure 5. Conductivity under redox cycling (air-H_2) at fixed temperature of sample LST-p-120.

In the beginning, when the sample is reduced at 1000 °C for 24 h, the apparent conductivity is 0.5 S/cm at 750 °C, and the sample showed a metallic behavior. Such a low value of conductivity was expected and was due to the high porosity introduced by graphite. The response to the atmosphere switch decreased the conductivity by about 4 orders of magnitude, and equilibrium was hardly reached, as suggested by hysteresis in the conductivity value after several cycles.

3.2. LST-Impregnated NiCrAl Foams

As mentioned in the previous paragraph, LST-c was chosen as the best powder to impregnate the NiCrAl foams and to study the composite material as a possible candidate for being a current collector in a metal-supported fuel cell. The study of LST-impregnated NiCrAl foams regarded two aspects of current collector: its chemical stability and its conductivity.

3.2.1. Chemical Stability

Before testing the chemical stability of LST-impregnated NiCrAl foams in real operative conditions as current collector, two intermediate experiments were performed to systematically study the chemical stability of the system, due to the formation of a layer of alumina on NiCrAl foams. The experiments are described in the following together with the results:

1. Study of pellets obtained by mixing of powders LST-c and Al_2O_3 after treatment at several different temperatures in air
2. Study of pellets obtained as a pre-sintered (1600 °C) fully dense Alumina core in a LST-c pellet after treatment at several different temperatures in air

The actual microstructure of the composite current collector is better described by experiment (2); nevertheless, in experiment (1), any possible reactivity phenomenon is emphasized because of higher surface density of powders. From experiment type (1) formation of new phases (due to reactivity of two powders) was not detected by XRD at any temperature. Peaks of measured patterns on mixed powders were compared with those of pure materials and reported in Figure 6, with Rietveld refinement. The lattice parameters, and some reliability factors of Rietveld Refinement are summarized in Table 4. Refinement was performed by considering both the two phases. From this table, it can be observed that the lattice parameter remains quite constant. Stability was confirmed by experiment (2), and no migration of elements was detected in LST or in alumina for all studied temperature at interface by EDAX analysis.

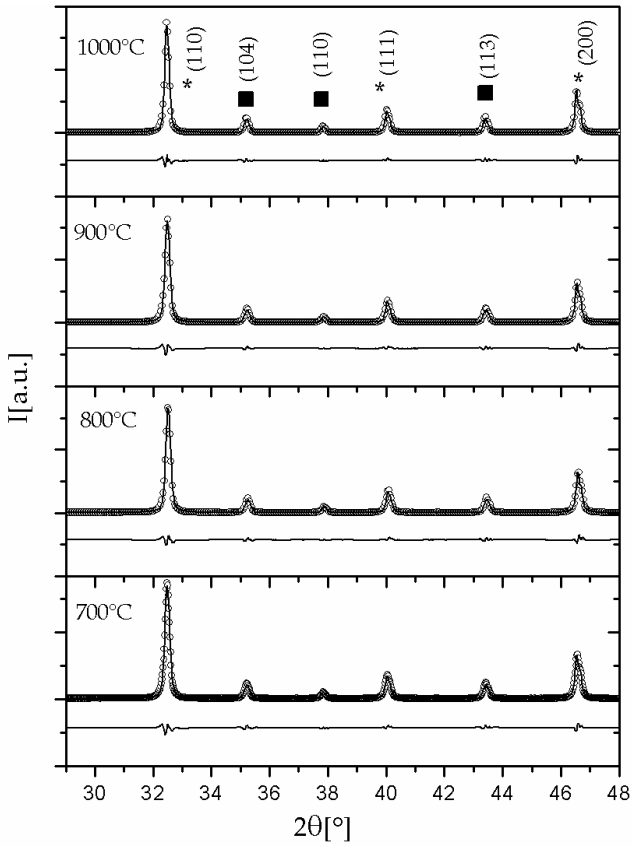

Figure 6. XRD patterns and Rietveld refinement of mixing of powders LST-c and Al_2O_3 after treatment in air at several different temperatures, as reported in the labels. Residuals and Miller indexes of Alumina (■) and LST (*) phases are also reported.

Table 4. Rietveld refined parameters of patterns reported in Figure 6.

Sample	Lattice Parameter (Å)	χ^2	R_B	R_F
Mixing at 700 °C	3.90051	3.8	2.52	1.78
Mixing at 800 °C	3.90026	3.5	2.68	2.13
Mixing at 900 °C	3.90058	2.8	2.22	1.84
Mixing at 1000 °C	3.90086	2.4	2.15	1.72

The same findings were detected by post-measurement analysis on the current collector composite, and a good stability, of both the ceramic impregnating material and the NiCrAl foam, was obtained in all conditions. In fact, as shown in Figure 7, after treatment at 750 °C for 300 h in H_2 the Al_2O_3 layer at the surface of the foam is still present, covering the entirety of the foam. Ni and Cr are confined inside the foam, although some segregation of Cr at the surface can be detected at a few points.

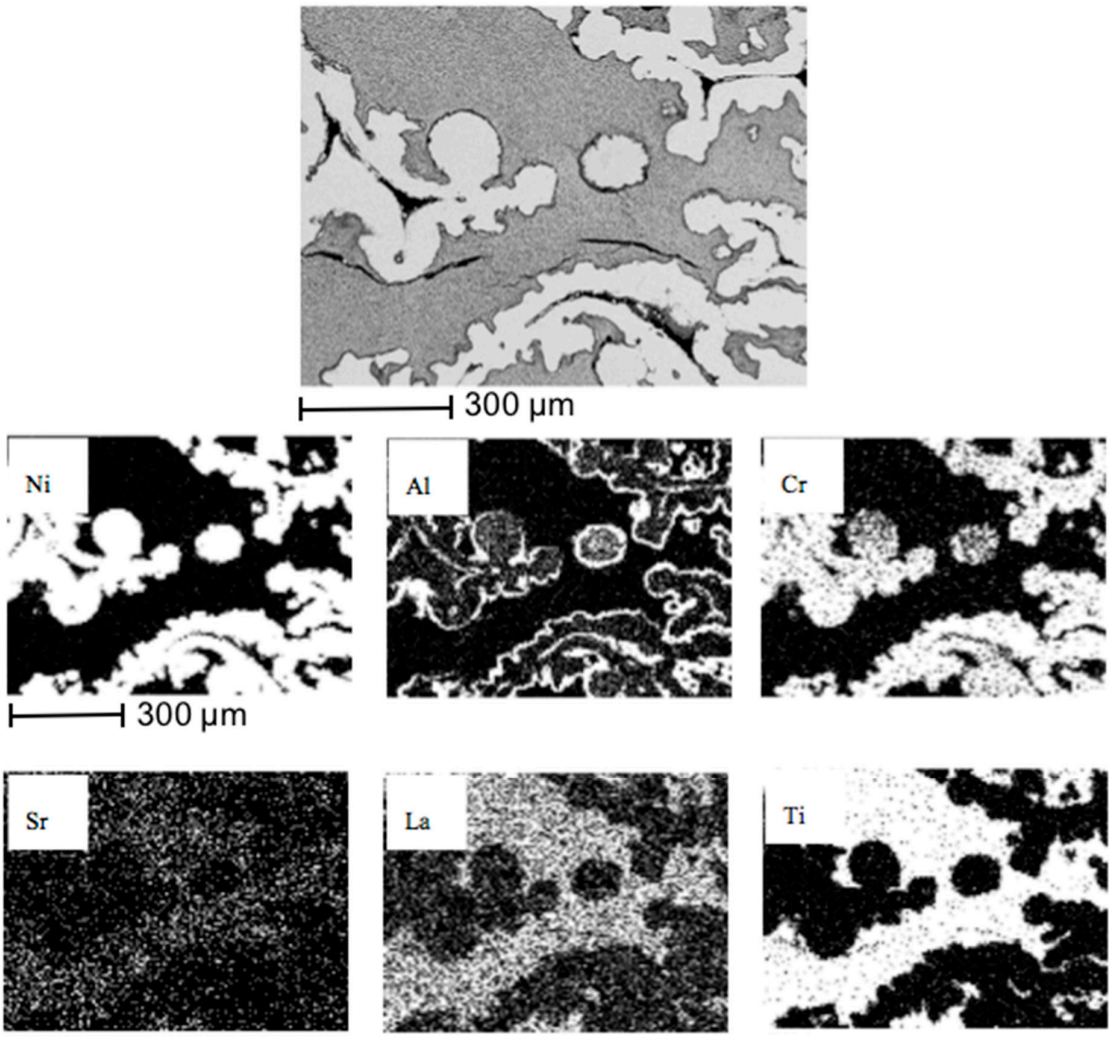

Figure 7. SEM+EDX maps of LST-NiCrAl current collector after reduction at 750 °C for 300 h.

One of these is shown in Figure 8, with spots of Cr oxide visible within the alumina layer. Diffusion of cations from ceramic components towards the foam was not detected, as Sr, La and Ti are only present in the core of the ceramic and do not react with Al.

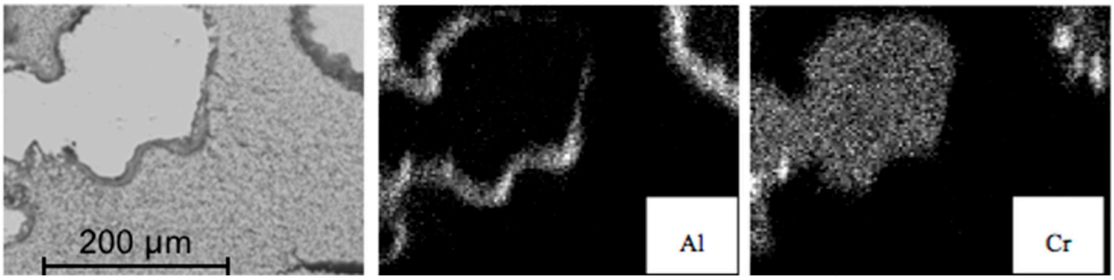

Figure 8. SEM+EDX maps of LST-NiCrAl current collector after reduction at 750 °C for 300 h: chromium segregation.

Very similar features (Figure 9) can be found after treatment at 900 °C and RedOx cycling (detailed treatment is reported in Figure 10b). In this case, no formation of Cr oxides is detected. From the above results on ceramics and composites, it can be concluded that LST is highly compatible with NiCrAl foams, and long-term operation without significant degradation can be expected.

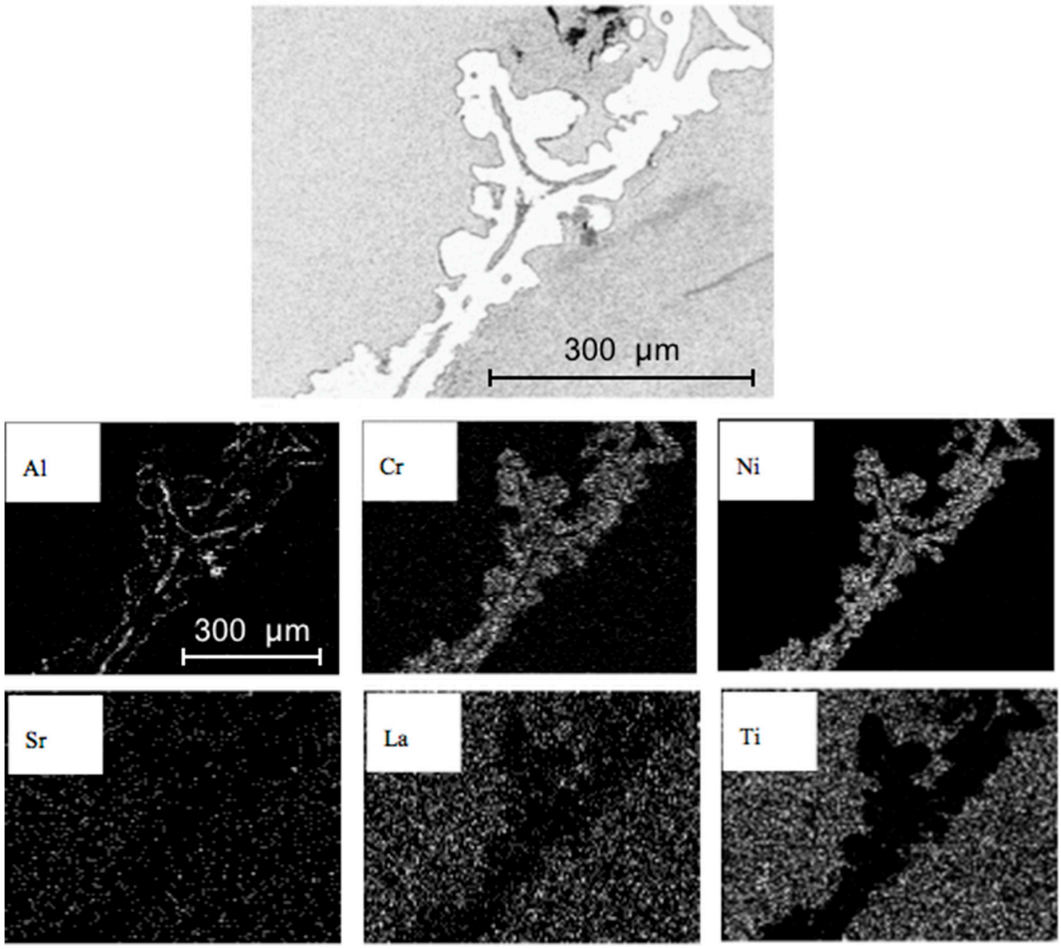

Figure 9. SEM+EDX maps of LST-NiCrAl current collector after treatment at 900 °C and RedOx cycling.

However, the reduction of LST requires high temperature—at least 900 °C—and high porosity—at least 30 vol %—as it was in composites presented here. Such requirements need to be carefully matched with constraints imposed by other parts of the cell and when robustness against RedOX cycling is required.

3.2.2. Conductivity

Conductivity of LST-impregnated NiCrAl foams reduced under H_2, was measured at two different temperatures, 750 and 900 °C, i.e., the operating temperature of the EVOLVE cell and the maximum temperature used for the cell fabrication. Results are reported in Figure 10. In general, the apparent conductivity is quite low due to the porosity (the current collector microstructure is reported in literature, ref [18]) and the lack of metallic electrodes. This was intentional in order to avoid short-circuiting with the metallic foam. At 750 °C (Figure 10a), reduction of the ceramic component is not yet completed after 300 h, and the behavior is substantially semiconducting as the conductivity drops by at least one order of magnitude on cooling. At 900 °C (Figure 10b), the sample reduces faster, but not completely after 20 h. Switching from H_2 to synthetic air produces huge conductivity change, by more than 3 orders, although equilibration appears very slow. Additionally, in this case an hysteresis in conductivity value after few cycles is observed.

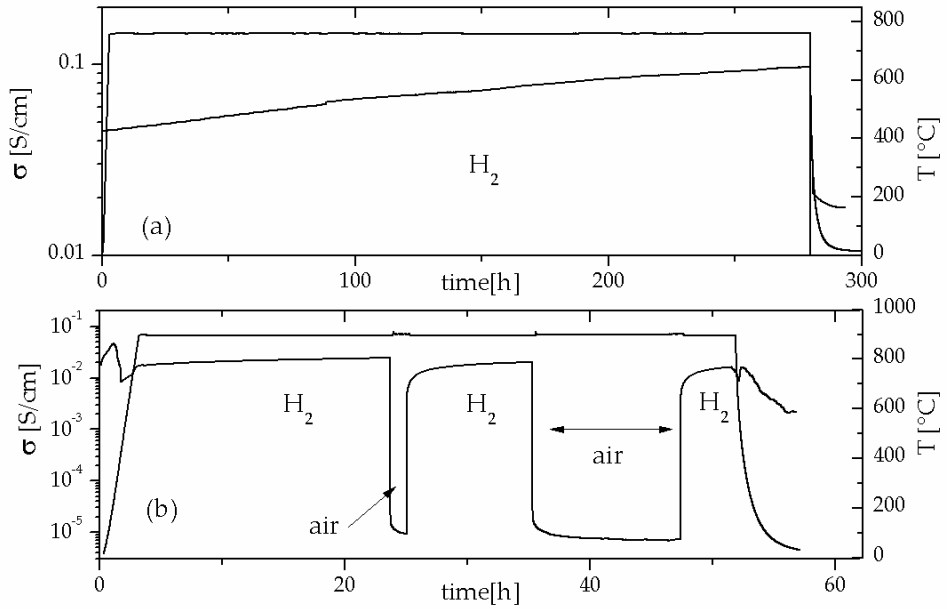

Figure 10. Conductivity of LST-impregnated NiCrAl foam at 750 °C (**a**) and 900 °C (**b**) under different atmospheres.

4. Discussion and Conclusions

Two different mechanisms of defect compensation, i.e., *electronic* at (*i*) low $P(O_2)$ and *cation vacancy type* at (*ii*) high $P(O_2)$, are assumed in donor-doped $SrTiO_3$ [38]. Incorporation mechanisms in La-doped $SrTiO_3$ can be described by the following reactions, respectively relevant for case (*i*) and (*ii*):

$$La_2O_3 + 2TiO_2 \xrightarrow{SrTiO_3} 2La_{Sr}^{\bullet} + 2Ti_{Ti}' + 6O_O^x + \frac{1}{2}O_2 \quad (1)$$

$$La_2O_3 + 3TiO_2 \xrightarrow{SrTiO_3} 2La_{Sr}^{\bullet} + V_{Sr}'' + 3Ti_{Ti}^x + 9O_O^x \quad (2)$$

where Kröger-Vink notation was used. As a result, the thermodynamically stable phase at low $P(O_2)$ is the conductive stoichiometric $Sr_{1-x}La_xTiO_3$, while at high $P(O_2)$ it is the insulating Sr-deficient $Sr_{1-1.5x}La_xTiO_3$. When the stoichiometric phase is exposed to oxidizing atmosphere, charge compensation changes from electronic to cation vacancy, causing the formation of secondary phases accommodating the Sr excess. Such phases were identified as SrO either precipitated at grain boundaries or present inside grains as shear planes [38,40] and can be hardly revealed at lower doping levels and by standard-resolution techniques. On the contrary, when the Sr-deficient phase is

subjected to reducing atmosphere, establishment of the electronic compensation imply accommodation of Ti excess by formation of TiO_2 Magneli phases either embedded in $SrTiO_3$ or as precipitate [40]. The process can be described as:

$$Sr_{1-1.5x}La_xTi^{4+}O_3 \xrightarrow{pO_2 \ll 1} Sr_{1-1.5x}La_xTi^{4+}_{1-1.5x}Ti^{3+}_xO_{3-1.5x} + \frac{x}{2}TiO_2 + \frac{x}{4}O_2 \quad (3)$$

The results presented about LST ceramics are in good agreement with the above-presented mechanisms: A-site deficient compositions (LST185 and LST27) did not show any secondary phase after sintering in air, and neither did LST-c after sintering in H_2. The application of reducing atmosphere promoted in LST185 and LST27 the formation of Ti-rich phase as indicated by Equation (3). Oxidation of LST-c did not reveal appearance of SrO-rich phases (see Figure 6) possibly due to kinetic limitations at moderate temperatures (T < 1000 °C).

Conductivity and activation energy values reported in Figure 3 suggest the existence of some ionic conduction, that could be explained by a mixed incorporation mode, i.e., by simultaneous formation of Sr and O vacancies, recently proposed for RE-doped $SrTiO_3$ [41].

Reduced materials showed metallic-type behavior (Figure 4) in any case. However, of A-site-deficient composition resulted in lower conductivity than in stoichiometric material, which is contrary to several reports. This might be explained by the presence of secondary phases in A-site-deficient LST and by the high temperature of reduction applied, as already reported in the literature [24]. The apparent inconsistency could be also ascribed to the different synthesis method used for stoichiometric (spray pyrolysis) and A-site-deficient (solid-state reaction) compositions, resulting in much finer and highly reactive powders in the first case.

Values of conductivity found in composites were limited by contact, which was intentionally not optimized in order to avoid possible side effects from metallic pastes.

In conclusion, the application of a composite material, the LST-impregnated NiCrAl foam, as a current collector in a metal-supported solid-oxide fuel cell was studied. For this purpose, the electronic properties of different compositions, stoichiometric and under stoichiometric, of LST were analyzed to choose the best one in terms of conductivity and phase purity. Then, LST chemical stability was studied in the presence of Al_2O_3 at different temperatures, gas compositions and aging times. Finally, stability and conductivity of the composite materials LST-impregnated NiCrAl foam were measured, and LST was found fully compatible with the NiCrAl foam, as no reactions were detected in oxidizing and reducing atmosphere after up to 300 h operation at 750 °C and 900 °C between the Al_2O_3 layer and LST. Results showed that the composite is suitable as current collector in the innovative design of metal-supported Solid Oxide Fuel Cells (SOFC), EVOLVE cells, in which the metallic part is supposed not only to provide the structural stability to the cell, but also to play the role of current collector due to the impregnation of the ceramic material.

Improvement in the layer performances might be obtained by using a LST-GDC-impregnated foam. The choice is motivated by the catalytic activity of GDC in the reduction of hydrogen, which should improve the total operation of the EVOLVE cell and by a better mechanical compatibility between the anodic part of the cell, the LST-GDC layer, and the GDC electrolyte.

Acknowledgments: The research leading to these results received funding from the European Union's Seventh Framework Programme (FP7/2007-2013) for the Fuel Cells and Hydrogen Joint Technology Initiative under grant agreement NO. 303429—EVOLVE. The authors are grateful to Alantum Europe GmbH, for supplying foams, and to Ceramic Powder Technology AS, for supplying commercial LST powders. Finally, the authors wish to thank F. Perrozzi for helping in doing measurements and Maria Teresa Buscaglia for synthesis of LST powders.

Author Contributions: All authors conceived, designed and performed the experiments; Sabrina Presto and Massimo Viviani analyzed the data and wrote the paper. Rémi Costa and Feng Han carried out foams impregnation.

Conflicts of Interest: The authors declare no conflict of interest.

References

1. Choudhury, A.; Chandra, H.; Arora, A. Application of solid oxide fuel cell technology for power generation—A review. *Renew. Sustain. Energy Rev.* **2013**, *20*, 430–442. [CrossRef]
2. Andersson, M.; Sundèn, B. *Technology Review—Solid Oxide Fuel Cell*; Report 2017:359; Energiforsk: Stockholm, Sweden, 2017; ISBN 978-91-7673-359-2. Available online: https://energiforskmedia.blob.core.windows.net/media/22411/technology-review-solid-oxide-fuel-cell-energiforskrapport-2017-359.pdf (accessed on 26 January 2018).
3. Massardo, A.F.; Lubelli, F. Internal Reforming Solid Oxide Fuel Cell-Gas Turbine Combined Cycles (IRSOFC-GT): Part A—Cell Model and Cycle Thermodynamic Analysis. *J. Eng. Gas Turbines Power* **1999**, *122*, 27–35. [CrossRef]
4. Ramadhani, F.; Hussain, M.A.; Mokhlis, H.; Hajimolana, S. Optimization strategies for Solid Oxide Fuel Cell (SOFC) application: A literature survey. *Renew. Sustain. Energy Rev.* **2017**, *76*, 460–484. [CrossRef]
5. Kendall, K.; Minh, N.Q.; Singhal, S.C. Chapter 8 Cell and Stack Designs. In *High-temperature Solid Oxide Fuel Cells: Fundamentals, Design and Applications*, 1st ed.; Singhal, S.C., Kendall, K., Eds.; Elsevier Science: London, UK, 2003; pp. 197–228; ISBN 9780080508085.
6. Mahmud, L.S.; Muchtar, A.; Somalu, M.R. Challenges in fabricating planar solid oxide fuel cells: A review. *Renew. Sustain. Energy Rev.* **2017**, *72*, 105–116. [CrossRef]
7. Su, S.; Gao, X.; Zhang, Q.; Kong, W.; Chen, D. Anode-Versus Cathode-Supported Solid Oxide Fuel Cell: Effect of Cell Design on the Stack Performance. *Int. J. Electrochem. Sci.* **2015**, *10*, 2487–2503.
8. Thorel, A.S.; Abreu, J.; Ansar, S.-A.; Barbucci, A.; Brylewski, T.; Chesnaud, A.; Ilhan, Z.; Piccardo, P.; Prazuch, J.; Presto, S.; et al. Proof of concept for the dual membrane cell I. Fabrication and electrochemical testing of first prototypes. *J. Electrochem. Soc.* **2013**, *160*, F360–F366. [CrossRef]
9. Presto, S.; Barbucci, A.; Viviani, M.; Ilhan, Z.; Ansar, S.-A.; Soysal, D.; Thorel, A.S.; Abreu, J.; Chesnaud, A.; Politova, T.; et al. IDEAL-Cell, innovative dual membrane fuel-cell: Fabrication and electrochemical testing of first prototypes. *ECS Trans.* **2009**, *25*, 773–782.
10. Xu, J.; Zhou, X.; Cheng, J.; Pan, L.; Wu, M.; Dong, X.; Sun, K. Electrochemical performance of highly active ceramic symmetrical electrode $La_{0.3}Sr_{0.7}Ti_{0.3}Fe_{0.7}O_{3-\delta}$-$CeO_2$ for reversible solid oxide cells. *Electrochim. Acta* **2017**, *257*, 64–72. [CrossRef]
11. Krishnan, V.V. Recent developments in metal-supported solid oxide fuel cells. *WIREs Energy Environ.* **2017**, *6*, e246. [CrossRef]
12. Zhou, Y.; Yuan, C.; Chen, T.; Meng, X.; Ye, X.; Li, J.; Wang, S.; Zhan, Z.J. Evaluation of Ni and Ni–$Ce_{0.8}Sm_{0.2}O_{2-\delta}$ (SDC) impregnated 430L anodes for metal-supported solid oxide fuel. *J. Power Sources* **2014**, *267*, 117–122. [CrossRef]
13. Blennow, P.; Sudireddy, B.R.; Persson, Å.H.; Klemensø, T.; Nielsen, J.; Thydén, K. Infiltrated $SrTiO_3$:FeCr-based Anodes for Metal-Supported SOFC. *Fuel Cells* **2013**, *13*, 494–505. [CrossRef]
14. Zhou, Y.; Meng, X.; Liu, X.; Pan, X.; Li, J.; Ye, X.; Nie, H.; Xia, C.; Wang, S.; Zhan, Z. Novel architectured metal-supported solid oxide fuel cells with Mo-doped $SrFeO_{3-\delta}$ electrocatalysts. *J. Power Sources* **2014**, *267*, 148–154. [CrossRef]
15. Matsuzaki, Y.; Yasuda, I. The poisoning effect of sulfur-containing impurity gas on a SOFC anode: Part I. Dependence on temperature, time, and impurity concentration. *Solid State Ion.* **2000**, *132*, 261–269. [CrossRef]
16. Khan, M.S.; Lee, S.-B.; Song, R.-H.; Lee, J.-W.; Lima, T.-H.; Park, S.-J. Fundamental mechanisms involved in the degradation of nickel–yttria stabilized zirconia (Ni–YSZ) anode during solid oxide fuel cells operation: A review. *Ceram. Int.* **2016**, *42*, 35–48. [CrossRef]
17. Choi, J.-J.; Ryu, J.; Hahn, B.-D.; Ahn, C.-W.; Kim, J.-W.; Yoon, W.-H.; Park, D.-S. Low temperature preparation and characterization of solid oxide fuel cells on FeCr-based alloy support by aerosol deposition. *Int. J. Hydrog. Energy* **2014**, *39*, 12878–12883. [CrossRef]
18. Han, F.; Semerad, R.; Constantin, G.; Dessemond, L.; Costa, R. Beyond the 3rd Generation of Planar SOFC: Development of Metal Foam Supported Cells with Thin Film Electrolyte. *ECS Trans.* **2015**, *68*, 1889–1896. [CrossRef]
19. Costa, R.; Ansar, A. Evolved Materials and Innovative Design for High Performance, Durable and Reliable SOFC Cell and Stack Presentation and Status of the European Project EVOLVE. *ECS Trans.* **2013**, *57*, 533–541. [CrossRef]

20. Marina, O.A.; Canfield, N.L.; Stevenson, J.W. Thermal, electrical, and electrocatalytical properties of lanthanum-doped strontium titanate. *Solid State Ion.* **2002**, *149*, 21–28. [CrossRef]
21. Verbraeken, M.C.; Ramos, T.; Agersted, K.; Ma, Q.; Savaniu, C.D.; Sudireddy, B.R.; Irvine, J.T.S.; Holtappels, P.; Tietz, F. Modified strontium titanates: From defect chemistry to SOFC anodes. *RSC Adv.* **2015**, *5*, 1168–1180. [CrossRef]
22. Canales-Vasquez, J.; Tao, S.W.; Irvine, J.T.S. Electrical properties in $La_2Sr_4Ti_6O_{19-delta}$: A potential anode for high temperature fuel cells. *Solid State Ion.* **2003**, *159*, 159–165. [CrossRef]
23. Savaniu, C.D.; Irvine, J.T.S. La-doped $SrTiO_3$ as anode materials for IT-SOFC. *Solid State Ion.* **2011**, *192*, 491–493. [CrossRef]
24. Burnat, D.; Heel, A.; Holzer, L.; Kata, D.; Lis, J.; Graule, T. Synthesis and Performances of A-site deficient lanthanum-doped strontium titanate by nanoparticle based spray pyrolysis. *J. Power Sources* **2012**, *201*, 26–36. [CrossRef]
25. Miller, D.N.; Irvine, J.T.S. B-site doping of lanthanum strontium titanate for solid oxide fuel cell anodes. *J. Power Sources* **2011**, *196*, 7323–7327. [CrossRef]
26. Zhou, X.; Yan, N.; Chuang, K.T.; Luo, J. Progress in La-doped $SrTiO_3$ (LST)-based anode materials for solid oxide fuel cells. *RSC Adv.* **2014**, *4*, 118–131. [CrossRef]
27. Yurkiv, V.; Constantin, G.; Hornes, A.; Gondolini, A.; Mercadelli, E.; Sanson, A.; Dessemond, L.; Costa, R. Towards understanding surface chemistry and electrochemistry of $La_{0.1}Sr_{0.9}TiO_{3-\alpha}$ based solid oxide fuel cell. *J. Power Sources* **2015**, *287*, 58–67. [CrossRef]
28. Gondolini, A.; Mercadelli, E.; Constantin, G.; Dessemond, L.; Yurkiv, V.; Costa, R.; Sanson, A. On the manufacturing of low temperature activated $Sr_{0.9}La_{0.1}TiO_{3-\delta}$-$Ce_{1-x}Gd_xO_{2-\delta}$ anode for solid oxide fuel cell. *J. Eur. Ceram. Soc.* **2018**, *38*, 153–161. [CrossRef]
29. Chen, G.; Kishimoto, H.; Yamaji, K.; Kuramoto, K.; Horita, T. Electrical performance of La-substituted $SrTiO_3$ anode material with different deficiencies in A-site. *ECS Trans.* **2013**, *50*, 63–71. [CrossRef]
30. Karczewski, J.; Riegel, B.; Molin, S.; Winiarski, A.; Gazda, M.; Jasinski, P.; Murawski, L.; Kusz, B. Electrical properties of $Y_{0.08}Sr_{0.92}Ti_{0.92}Nb_{0.08}$ $O_{3-\delta}$ after reduction in different reducing conditions. *J. Alloys Compd.* **2009**, *473*, 496–499. [CrossRef]
31. Ishihara, T.; Matsuda, H.; Bustam, M.A.B.; Takita, Y. Oxide ion conductivity in doped Ga based perovskite type oxide. *Solid State Ion.* **1996**, *86–88*, 197–201. [CrossRef]
32. Slater, P.R.; Irvine, J.T.S.; Ishihara, T.; Takita, Y. High-Temperature Powder Neutron Diffraction Study of the Oxide Ion Conductor $La_{0.9}Sr_{0.1}Ga_{0.8}Mg_{0.2}O_{2.85}$. *J. Solid State Chem.* **1998**, *139*, 135–143. [CrossRef]
33. Slater, P.R.; Fagg, D.P.; Irvine, J.T.S. Synthesis and electrical characterization of doped perovskite titanates as potential anode materials for solid oxide fuel cells. *J. Mater. Chem.* **1997**, *7*, 2495–2498. [CrossRef]
34. Savaniu, C.; Irvine, J.T.S. Reduction studies and evaluation of surface modified A-site deficient La-doped $SrTiO_3$ as anode material for IT-SOFCs. *J. Mater. Chem.* **2009**, *19*, 8119–8128. [CrossRef]
35. Hui, S.; Petric, A. Evaluation of yttrium-doped $SrTiO_3$ as an anode for solid oxide fuel cells. *J. Eur. Ceram. Soc.* **2002**, *22*, 1673–1681. [CrossRef]
36. Hui, S.; Petric, A. Electrical Properties of Yttrium-Doped Strontium Titanate under Reducing Conditions. *J. Electrochem. Soc.* **2002**, *149*, J1–J10. [CrossRef]
37. Hui, S.; Petric, A. Electrical conductivity of yttrium-doped $SrTiO_3$: Influence of transition metal additives. *Mater. Res. Bull.* **2002**, *37*, 1215–1231. [CrossRef]
38. Kolodiazhnyi, T.; Petric, A. The Applicability of Sr-deficient n-type $SrTiO_3$ for SOFC Anodes. *J. Electroceram.* **2005**, *15*, 5–11. [CrossRef]
39. Blennow, P.; Hansen, K.K.; Wallenberg, L.R.; Mogensen, M. Effects of Sr/Ti-ratio in $SrTiO_3$-based SOFC anodes investigated by the use of cone-shaped electrodes. *Electrochim. Acta* **2006**, *52*, 1651–1661. [CrossRef]
40. Cumming, D.J.; Kharton, V.V.; Yaremchenko, A.A.; Kovalevsky, A.V.; Kilner, J.A. Electrical Properties and Dimensional Stability of Ce-Doped $SrTiOO_{3-\delta}$ for Solid Oxide Fuel Cell Applications. *J. Am. Ceram. Soc.* **2011**, *94*, 2993–3000. [CrossRef]
41. Zulueta, Y.A.; Dawson, J.A.; Mune, P.D.; Froeyen, M.; Nguyen, M.T. Oxygen vacancy generation in rare-earth-doped $SrTiO_3$. *Phys. Status Solidi (b)* **2016**, *253*, 2197–2203. [CrossRef]